JACS
JOURNAL OF THE AMERICAN CHEMICAL SOCIETY

Article

pubs.acs.org/JACS

Molecular Dynamics Simulations Reveal a Dielectric-Responsive Coronal Structure in Protein−Polymer Surfactant Hybrid Nanoconstructs

Alex P. S. Brogan,[†] Richard B. Sessions,[‡] Adam W. Perriman,*[,†,§] and Stephen Mann*[,†]

[†]Centre for Organized Matter Chemistry and Centre for Protolife Research, School of Chemistry, University of Bristol, Bristol BS8 1TS, U.K.

[‡]School of Biochemistry, University of Bristol, Bristol BS8 1TD, U.K.

[§]School of Cellular and Molecular Medicine, University of Bristol, Bristol BS8 1TD, U.K.

Supporting Information

ABSTRACT: Solvent-free liquid proteins are a new class of thermally stable hybrid bionanomaterials that are produced by extensive lyophilization of aqueous solutions of protein−polymer surfactant nanoconjugates followed by thermal annealing. The hybrid constructs, which consist of a globular protein core surrounded by a monolayer of electrostatically coupled polymer surfactant molecules, exhibit nativelike structure, function, and backbone dynamics over a large temperature range. Despite the key importance of the polymer surfactant shell, very little is known about the atomistic structure of the corona and how it influences the phase behavior and properties of these novel nanoscale objects. Here we present molecular dynamics simulations of protein−polymer surfactant nanoconjugates consisting of globular cores of myoglobin or lysozyme and demonstrate that the derived structural parameters are highly consistent with experimental values. We show that the coronal layer structure is responsive to the dielectric constant of the medium and that the mobility of the polymer surfactant molecules is significantly hindered in the solvent-free state, providing a basis for the origins of retained protein dynamics in these novel biofluids. Taken together, our results suggest that the extension of molecular dynamics simulations to hybrid nanoscale objects could be of generic value in diverse areas of soft matter chemistry, bioinspired engineering, and biomolecular nanotechnology.

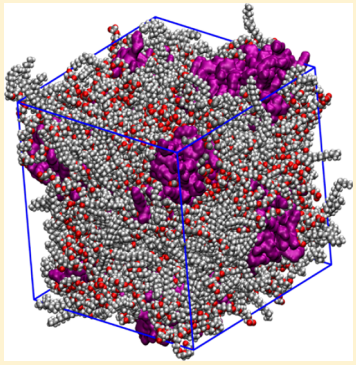

INTRODUCTION

Versatile and robust methods for extracting structural information are key requirements for understanding the emergent properties of soft matter and providing a reliable framework for the rational design of new functional materials. In this regard, a description of the atomistic structure of soft matter is often difficult to determine experimentally because of the intrinsically disordered states adopted by many of these types of materials. Accordingly, small-angle X-ray and neutron scattering techniques are often employed to gain insight into the internal structure of soft materials, although these techniques supply limited information at atomic resolution and transformations from reciprocal space to real space for structure elucidation often rely on various assumptions. The need for molecular dynamics simulations is therefore of paramount importance in interpreting a wide range of experimental observations, correlating the relationships between structure and function, and providing guidelines for the design of new materials and systems.[1−3]

Molecular dynamics simulations are currently being employed to elucidate the structure and formation of large-scale biomolecular assemblies such as amyloid fibers[4,5] and protein−lipid membrane ensembles[6−9] as well as a range of self-assembled de novo proteins.[10−12] Despite these advances, the development of molecular dynamics simulations for the elucidation of nanoscale objects comprising integrated hybrid components appears to be relatively unexplored, even though such constructs are of key importance in soft matter chemistry and physics. Studies of protein−polymer interactions[13,14] and enzyme nanogels[15] have been undertaken, but there appear to be very few reports of molecular dynamics simulations of protein-based hybrid nano-objects. Herein we present to the best of our knowledge the first example of the use of molecular dynamics to elucidate the atomistic structure of discrete protein−polymer surfactant nanoscale conjugates dispersed in aqueous or nonaqueous solvents or in the form of a single-phase solvent-free liquid.

We recently developed an unprecedented approach for the synthesis of a new type of soft matter based on protein−polymer surfactant nanoscale conjugates that exist as solvent-free solids and liquids under ambient conditions.[16] Significantly, the globular protein molecules are surrounded by an electrostatically attached polymer surfactant corona, which in the absence of a solvent extends the range of the interparticle interactions between the hybrid nano-objects. As a conse-

Received: July 30, 2014
Published: November 7, 2014

dx.doi.org/10.1021/ja507592b | J. Am. Chem. Soc. 2014, 136, 16824−16831

quence, lyophilization of the aqueous nanoconjugates produces a solvent-free soft solid that melts at close to room temperature to give a viscous solvent-free liquid phase containing intact protein−polymer surfactant conjugates and very low numbers of structurally associated water molecules. Our previous reports on myoglobin[17−20] and lysozyme[21] protein melts have indicated that the protein globular structure and conformational freedom are retained in the solvent-free state. As a consequence, reversible dioxygen binding was observed for the solvent-free liquid myoglobin.[17] Moreover, the highly constricted molecular environment associated with the solvent-free liquids results in unprecedented thermal stability of the protein structure.[18,21] For example, the half-denaturation temperature associated with lysozyme in the solvent-free liquid state was 178 °C.[21] The unfolding mechanism shifted from a classical two-state pathway observed for lysozyme in water to a three-state denaturation profile involving a stabilized intermediate in the solvent-free melt.[21]

Significantly, elastic incoherent neutron scattering (EINS) demonstrated that the protein dynamics associated with a myoglobin−polymer surfactant conjugate present in the solvent-free liquid state closely resembled those observed in water, indicating that the polymer surfactant corona was able to dynamically replace water and act as a surrogate solvent.[19] Determining the conformation of the polymer surfactant corona in both the aqueous phase and the subsequently restrictive environment of the solvent-free liquid is critical for understanding the behavior of these unusual solvent-free biofluids and designing new biomolecular systems based on the experimental methodologies. Low-resolution details of the coronal structure were recently obtained from dynamic light scattering studies and small-angle scattering.[21] Herein we undertake a series of molecular dynamics simulations on lysozyme and myoglobin in both the aqueous and solvent-free states to elucidate the structure of the polymer surfactant corona at the atomistic level. The simulations are compared with experimental data obtained from small-angle neutron scattering (SANS).

Our results indicate that the structural parameters associated with the atomistic models of the protein−polymer surfactant nanoconstructs are highly reminiscent of experimental data obtained for these systems. We show that molecular dynamics simulations can be used to describe the structure of the polymer surfactant corona in aqueous, nonaqueous, and solvent-free environments. Specifically, the simulations demonstrate that the average head-to-tail distance of the polymer surfactant molecules in the solvent-free state is increased or decreased compared with simulations undertaken in the presence of water or acetonitrile, respectively. This unprecedented insight into the coronal structure could aid significantly in predicting how molecules such as enzymatic substrates and products might interact with the solvent-free liquid proteins. In addition, these simulations reveal that the lability of polymer surfactant molecules is significantly hindered in the solvent-free liquid, providing a basis for the origin of the retained protein dynamics in these novel biofluids.

RESULTS AND DISCUSSION

Preparation of the solvent-free liquid proteins was undertaken using a three-step protocol involving (i) cationization of native lysozyme or myoglobin in water by carbodiimide-mediated coupling of *N*,*N*′-dimethyl-1,3-propanediamine (DMPA) to accessible carboxylic acid side chains, (ii) electrostatic binding of a stoichiometric amount of the anionic polymer surfactant glycolic acid ethoxylate lauryl ether (S_2) (M_w = 757 g·mol^{-1}; Figure 1a) to the cationized proteins (C-Lyz, C-Mb) to produce an aqueous solution of protein−polymer surfactant nanoconjugates ([C-Lyz][S_2], [C-Mb][S_2]), and (iii) extensive dehydration and thermal annealing of the [C-Lyz][S_2] and [C-Mb][S_2] soft solids to generate solvent-free protein liquids.

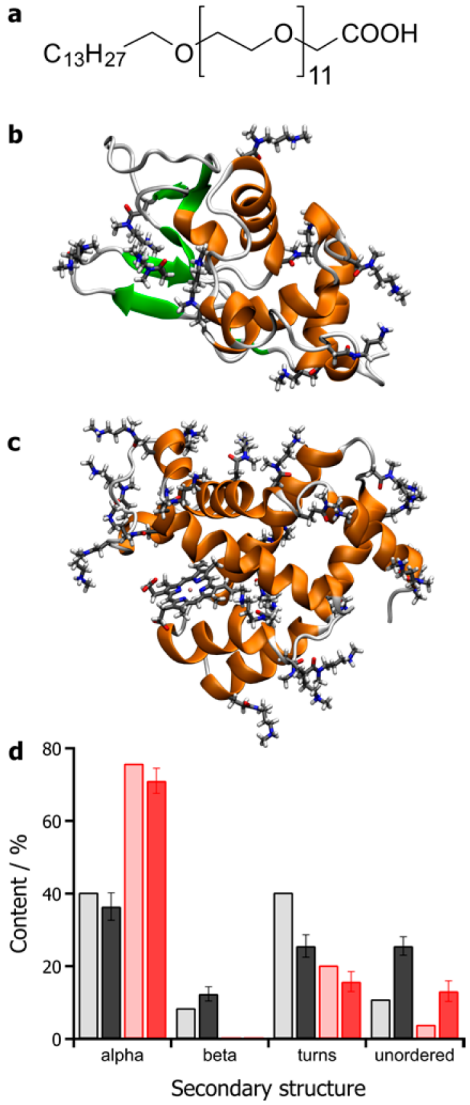

Figure 1. (a) Chemical structure of S_2 (as supplied by Sigma). (b, c) Molecular models showing the secondary structure and DMPA-modified side chains of Asp and Glu for C-Lyz (b) and C-Mb (c) after 100 ns of molecular dynamics simulation. (d) Secondary structure content for C-Lyz (black) and C-Mb (red) after 100 ns of simulation (error bars are standard deviations determined from the last 20 ns of simulation). For reference, the secondary structure contents for Lyz (gray) and Mb (light red) are also shown (calculated from crystal structures 2VB1 and 2VLY, respectively, using PDBsum).

Given this experimental methodology, we first performed energy minimization and molecular dynamics simulations of the cationized forms of lysozyme and myoglobin by using the corresponding Protein Data Bank (PDB) structures (myoglobin, 2VLY;[22] lysozyme, 2VB1[23]) and exchanging the Asp and Glu residues for equivalents modified with DMPA (Figure 1b,c). The simulated secondary structures (Figure 1d) were

dx.doi.org/10.1021/ja507592b | J. Am. Chem. Soc. 2014, 136, 16824−16831

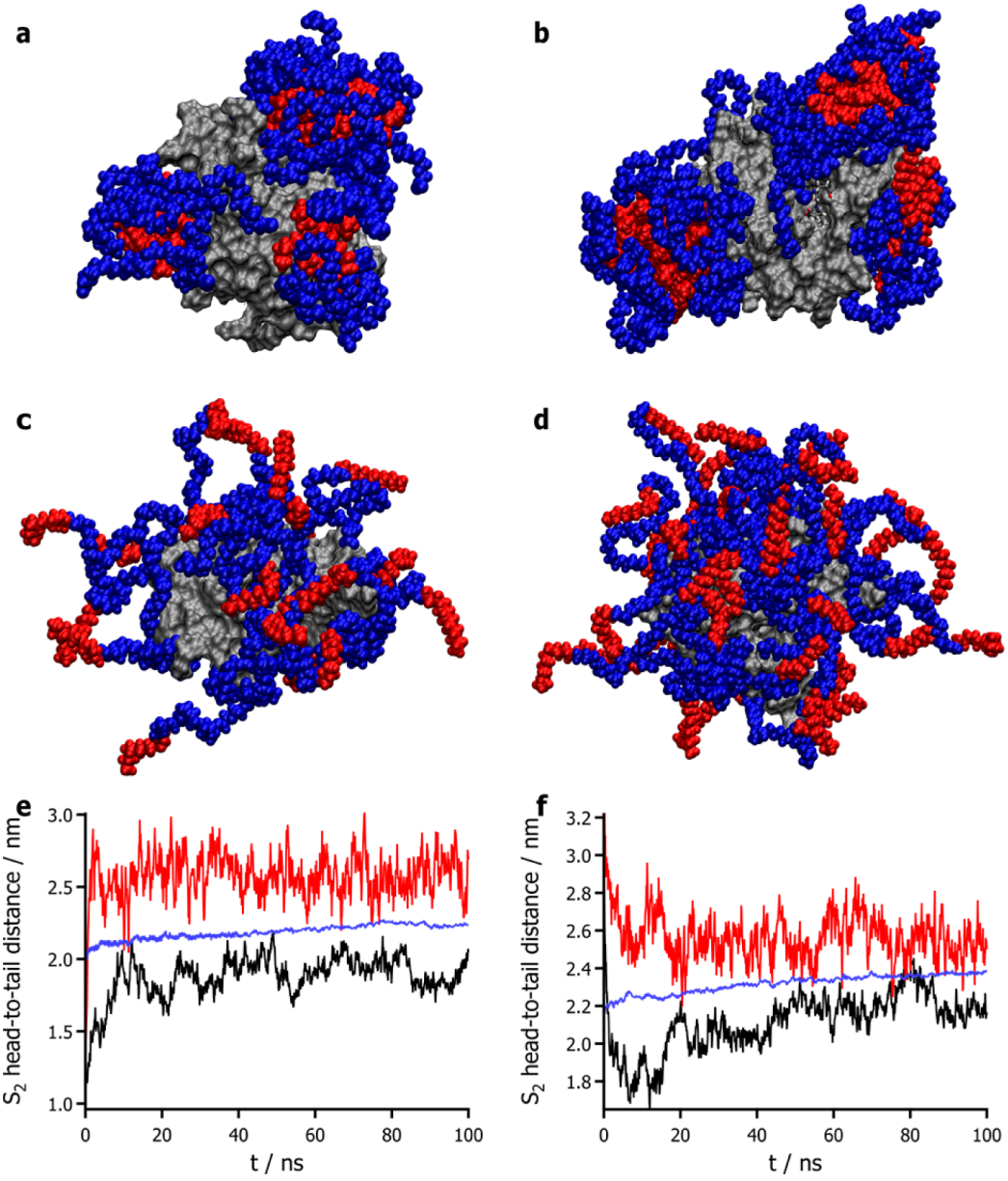

Figure 2. (a–d) Molecular models showing the arrangements of S_2 molecules after 100 ns of simulation for [C-Lyz][S_2] and [C-Mb][S_2] nanoconjugates in water (a and b, respectively) and acetonitrile (c and d, respectively). Blue and red indicate hydrophilic PEG groups and hydrophobic alkyl chains, respectively, associated with the polymer surfactant; gray indicates solvent-accessible sites on the surface of the cationized protein. (e, f) Plots of S_2 head-to-tail distance across the 100 ns molecular dynamics simulations in water (black), acetonitrile (red), and solvent-free (blue) for [C-Lyz][S_2] (e) and [C-Mb][S_2] (f).

consistent with experimentally derived data obtained from synchrotron radiation circular dichroism spectra of samples of C-Lyz[21] and C-Mb[17,18] and showed α-helix/β-sheet compositions of 36/12% and 71/0%, respectively. Here the influence of increasing the positive surface charge density on the secondary structure of the cationized proteins is consistent with a strong dependence of the globular architectures on inter- and intrahelix electrostatic stabilization,[24,25] which involves glutamic and aspartic acid side chains that are targeted in the cationization process. Plots of the root-mean-square deviation (RMSD) in the protein atomic positions against simulation time approach convergence to values between 0.2 and 0.3 nm (Supporting Information (SI) Figure 1), indicating that stable structures were observed within 100 ns for both C-Lyz and C-Mb. This was further confirmed by the minimal deviations from the initial structure after 100 ns in the secondary structure (SI Figures 2 and 3), number of hydrogen bonds (SI Figure 4), and solvent-accessible surface area (SI Figure 5).

Taken together, the above results provided initial validation of the molecular models and force fields used to describe the simulation of the cationized proteins over a 100 ns time scale. We therefore extended our methodology to the construction of stoichiometric protein–polymer surfactant nanoconjugates ([C-Lyz][S_2] and [C-Mb][S_2]) by docking the required number of S_2 molecules to the surface of the cationized proteins to generate charge neutrality (26 S_2 for C-Lyz and 43 S_2 for C-Mb). The hybrid constructs were then energy-minimized and subjected to 100 ns of molecular dynamics simulations in water (Figure 2a,b). Low deviations in the protein secondary structure (SI Figures 2 and 3), number of

dx.doi.org/10.1021/ja507592b | J. Am. Chem. Soc. 2014, 136, 16824–16831

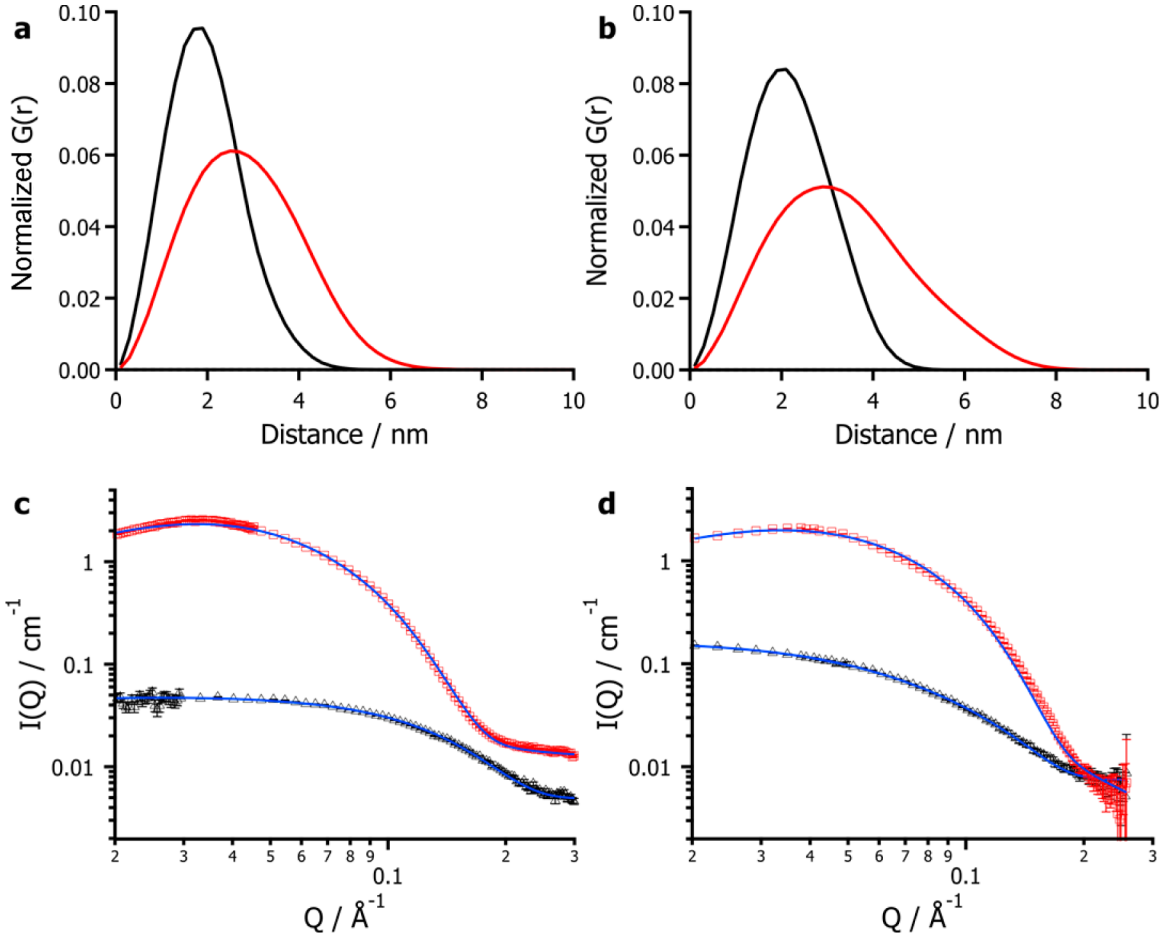

Figure 3. (a, b) Plots of the normalized radial distribution function $G(r)$ against distance for (a) aqueous C-Lyz (black) and aqueous [C-Lyz][S_2] (red) and (b) aqueous C-Mb (black) and aqueous [C-Mb][S_2] (red) averaged over a 100 ns simulation trajectory. The maximum peak intensity corresponds to the average spherical radius of the molecule. (c, d) Small-angle neutron scattering profiles for (c) aqueous C-Lyz (black triangles) and aqueous [C-Lyz][S_2] (red squares) and (d) Aqueous C-Mb (black triangles) and [C-Mb][S_2] (red squares) fitted to a Gaussian sphere model and a core−shell model for cationized and conjugated species, respectively (blue lines). For aqueous [C-Lyz][S_2], the radius of C-Lyz was kept constant at 1.40 nm, resulting in a shell thickness of 1.54 nm. For aqueous [C-Mb][S_2], the radius of C-Mb was kept constant at 1.93 nm, resulting in a shell thickness of 0.79 nm. In all cases, the fits proceeded with errors of <1%. The aqueous [C-Lyz][S_2] data were reported in a previous publication as supporting information.[21]

hydrogen bonds (SI Figure 4), and solvent-accessible surface area (SI Figure 5) coupled with the approach of the RMSD to convergence (SI Figure 1) indicated that the equilibrium secondary structure of the protein core was retained in each simulated hybrid nanoconjugate. Moreover, the polymer surfactant molecules adopted stable conformations throughout the simulation and became organized dynamically on the protein surface into micellelike clusters in which the hydrophobic alkyl tail and hydrophilic poly(ethylene oxide) segments were buried and exposed, respectively (Figure 2a,b). We attributed the surface reconstruction of the coronal layer to the high dielectric constant of the simulated medium. This was in agreement with molecular dynamics simulations conducted in a dipolar aprotic solvent (acetonitrile[26]), which displayed a coronal layer with the hydrophobic alkyl tail segments extended away from the protein surface (Figure 2c,d). The results indicated that the coronal structure could be assembled onto the protein surface without disruption of the embedded globular structure. Moreover, the structure adopted by the polymer surfactant shell was highly sensitive to the dielectric constant of the surrounding medium. To quantify this, the average distances between the ends of the S_2 molecules throughout the simulations were calculated (Figure 2e,f). As a result of hydrophobic tail burial, the equilibrium S_2 head-to-tail distances in water were 1.9 ± 0.08 and 2.2 ± 0.05 nm for [C-Lyz][S_2] and [C-Mb][S_2], respectively. By comparison, the equilibrium S_2 head-to-tail distances for [C-Lyz][S_2] and [C-Mb][S_2] in acetonitrile were 2.6 ± 0.1 and 2.5 ± 0.08 nm, respectively, reflecting the more extended architecture of the coronal layer in nonaqueous environments. These observations were consistent with experimental data on the observed solubility of the myoglobin−polymer surfactant conjugates in a range of aqueous and nonaqueous solvents.[27]

The radii of the simulated [C-Lyz][S_2] and [C-Mb][S_2] hybrid constructs in water were determined to be 2.62 and 2.88 nm, respectively, by using the peak intensity of the normalized radial distribution function $G(r)$, which was obtained from the calculated structure factor using *g_sans* as a measure of the spherical radius of the system (Figure 3a,b). The radii, which were 0.81 and 0.85 nm larger than the radii determined for the cationized proteins (Figure 3a,b and Table 1), were in agreement with values determined experimentally from fits to SANS data (2.94[21] and 2.72 nm for [C-Lyz][S_2] and [C-Mb][S_2], respectively; Figure 3c,d and Table 1).

dx.doi.org/10.1021/ja507592b | J. Am. Chem. Soc. 2014, 136, 16824−16831

Table 1. Radii of Aqueous C-Lyz, Aqueous [C-Lyz][S_2], C-Mb, and Aqueous [C-Mb][S_2] As Determined in Silico (Peak $G(r)$ Calculated Using *g_sans*) and Experimentally Using SANS

	r/nm	
	$G(r)$	SANS
C-Lyz	1.81	1.40
[C-Lyz][S_2]	2.62	2.94
C-Mb	2.03	1.93
[C-Mb][S_2]	2.88	2.72

Given the closeness of the computed and measured radii, we were confident that the molecular dynamics simulations gave realistic atomistic structures of the protein−polymer surfactant nanoconjugates immersed in a solvent-containing (aqueous) medium. We therefore developed our approach to the simulation of the solvent-free liquid state of the hybrid nanoconjugates in order to advance our understanding of these novel nanostructured biofluids. For this, eight copies of the simulated [C-Lyz][S_2] or [C-Mb][S_2] constructs were placed into a periodic box that was subsequently relaxed under simulated pressure (100 bar) to bring the nanoconjugates close together. The condensed system was then simulated at 298 K for 100 ns, followed by simulated annealing at 338 K (Figure 4a,b), which is above the melting temperatures observed experimentally for [C-Lyz][S_2] (294 K) and [C-Mb][S_2] (299 K). Plots of simulation volume against simulation time showed that [C-Lyz][S_2] and [C-Mb][S_2] were fully equilibrated after 100 and 50 ns, respectively (SI Figure 6). In addition, comparable to the aqueous simulations, the low deviations in secondary structure (SI Figures 2 and 3), number of hydrogen bonds (SI Figure 4), and solvent-accessible surface area (SI Figure 5) indicated that the myoglobin and lysozyme structures remained intact throughout the molecular dynamics simulations. This was in agreement with experimental observations for solvent-free liquid [C-Lyz][S_2] and [C-Mb][S_2].[17,18,21] The simulations revealed a structure for the solvent-free liquids in

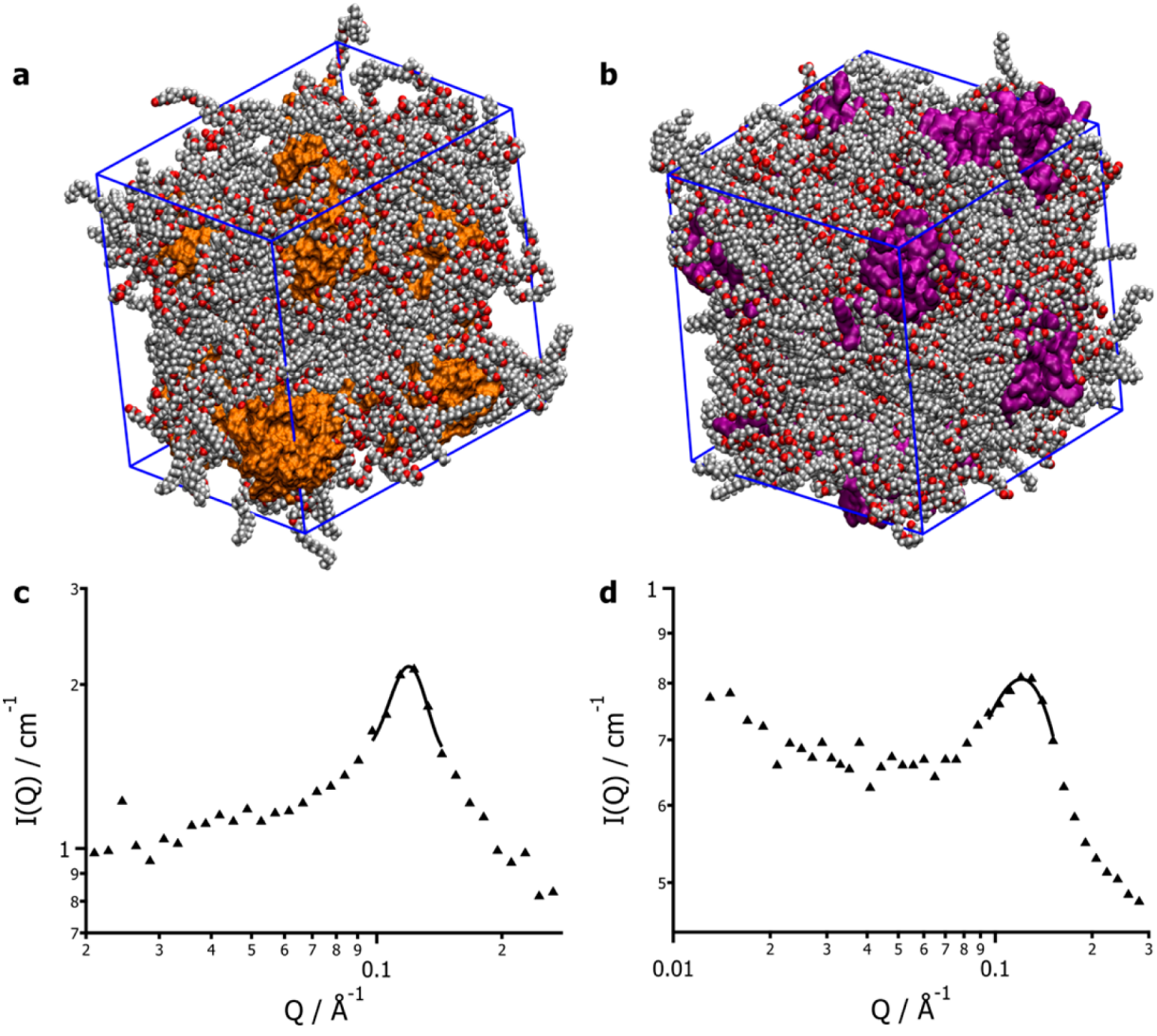

Figure 4. (a, b) Molecular models showing condensed arrays of eight repeats of solvent-free [C-Lyz][S_2] (a) and [C-Mb][S_2] (b) after simulated annealing at 338 K for 100 and 50 ns, respectively. Solvent-accessible regions of the protein surface are shown in orange and purple for C-Lyz and C-Mb, respectively. Polymer surfactant molecules are shown by van der Waals radii (C = gray, H = white, O = red), and the periodic boundary is shown in blue. (c, d) Small-angle neutron scattering profiles for solvent-free liquid [C-Lyz][S_2] (c) and [C-Mb][S_2] (d) at 30 °C, showing protein−protein correlation distances fitted with a Gaussian distribution. The lysozyme data were published in a previous article.[21]

dx.doi.org/10.1021/ja507592b | J. Am. Chem. Soc. 2014, 136, 16824−16831

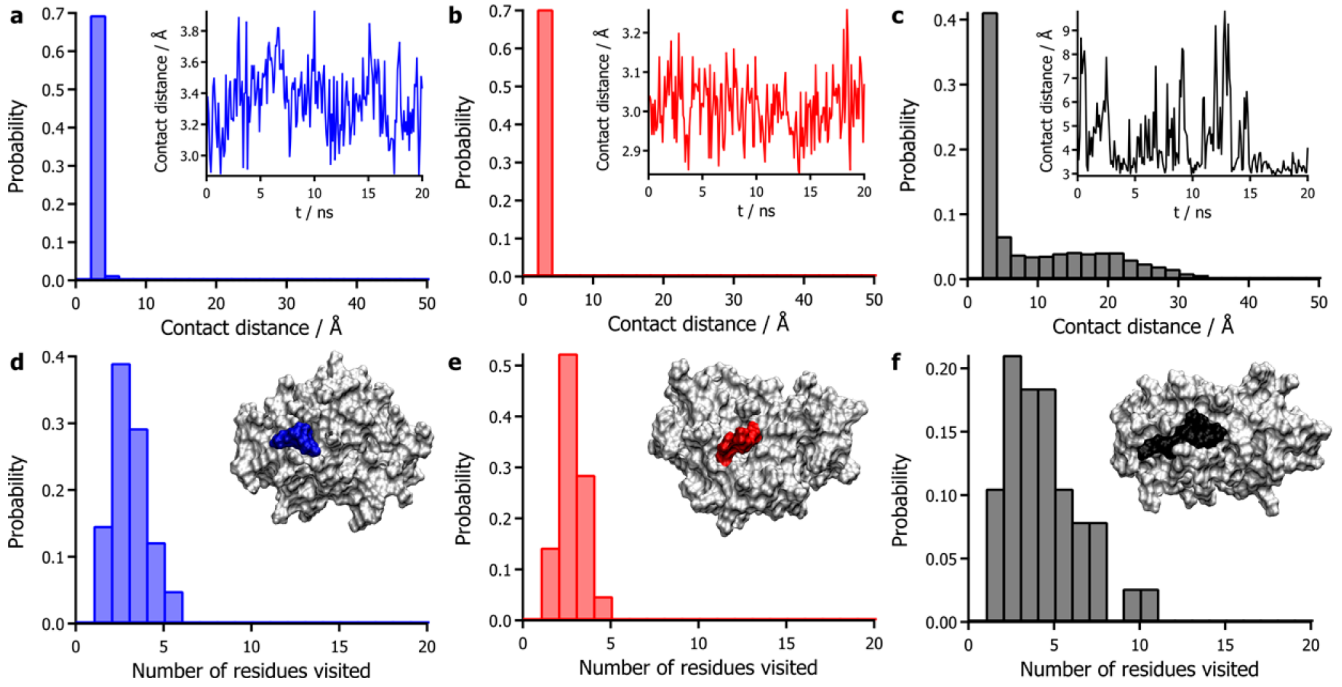

Figure 5. (a–c) Probability distributions of the contact distance between the carboxylate of S_2 molecules and the protein surface over the last 20 ns (recorded every 100 ps) of the respective simulations for [C-Mb][S_2] in the solvent-free phase (a), acetonitrile (b), and water (c). The insets show representative examples of the contact distance over the last 20 ns of the simulation period. (d–f) Probability distributions of the number of amino acid residues encountered (within 8 Å) per S_2 molecule over the last 20 ns (recorded every 100 ps) of the respective simulations for [C-Mb][S_2] in the solvent-free phase (d), acetonitrile (e), and water (f). In the insets, the highlighted residues on the surface of C-Mb are ones that were encountered by a representative S_2 molecule in the last 20 ns of the simulation period.

which the closely packed proteins were separated by relatively compressed surfactant coronas. Further examination of the equilibrium structures (SI Figure 7) revealed that both [C-Lyz][S_2] and [C-Mb][S_2] remained as a single phase of discrete nanoconjungates in the solvent-free melt. Significantly, no detachment of the polymer surfactant corona from the associated protein core was observed over the duration of the simulation. Moreover, the structure of the compacted polymer surfactant corona consisted of a homogeneous distribution of relatively extended and disordered chains that emanated from the protein surface and exhibited a degree of low-level interdigitation with S_2 molecules attached to neighboring nanoconstructs. In addition, the coronal conformation closely resembled that determined for simulations undertaken in a low-dielectric medium (Figure 2c,d). The equilibrium head-to-tail distances of the S_2 molecules were 2.2 ± 0.01 and 2.4 ± 0.007 nm for [C-Lyz][S_2] and [C-Mb][S_2], respectively (Figure 2e,f). These values were intermediate between those determined for the aqueous and acetonitrile simulations, signifying that the corona was less polar than water but more polar than acetonitrile.

The average nearest-neighbor center-to-center separations were 4.5 ± 0.1 and 4.8 ± 0.1 nm for the simulated [C-Lyz][S_2] and [C-Mb][S_2] solvent-free liquids, respectively. These separations are shorter than corresponding values obtained from SANS (5.3 nm (0.119 $Å^{-1}$)[21] and 5.1 nm (0.122 $Å^{-1}$) for [C-Lyz][S_2] and [C-Mb][S_2], respectively; Figure 4c,d). The observed discrepancy between the simulations and SANS measurements was attributed primarily to the polydispersity in the molecular weight of the polymer surfactant. While a value of 757 g·mol^{-1} was used for the molecular modeling, MALDI mass spectrometry showed that the polymer had a broad population of molecular weights, with a number-average molecular weight of 856 g·mol^{-1} (SI Figure 8).

Analysis of the molecular dynamics trajectories with respect to the amino acid residue closest to the carboxylate headgroup of S_2 revealed that during the last 20 ns of the simulations (representative of the equilibrated system) the average separations between the S_2 headgroup and the nearest amino acid were 3.2 ± 0.3 and 3.2 ± 0.2 Å for [C-Mb][S_2] (Figure 5a) and [C-Lyz][S_2] (SI Figure 9), respectively. This indicated that the extended polymer surfactant molecules remained strongly adhered to the surface of the protein in the solvent-free liquid. A similar level of immobilization was observed in the simulations of the protein–polymer surfactant nanoconstructs in acetonitrile, which gave average S_2–protein separations of 3.2 ± 0.2 Å for [C-Mb][S_2] (Figure 5b) and [C-Lyz][S_2] (SI Figure 9).

In contrast, the nearest-neighbor contacts between the protein and polymer surfactant molecules in water showed that the S_2 molecules were significantly more labile (Figure 5c and SI Figure 9). Although the majority of recorded separations were similar to those observed in acetonitrile and the solvent-free state, there was the additional presence of a broad range of separations. These observations were extended by investigating the number of amino acid residues in contact with individual surfactant molecules to provide a measure of lateral movement across the protein surface (Figure 5d–f and SI Figure 9). In the solvent-free liquid, the S_2 headgroups were in contact with on average 2.5 ± 1 and 3 ± 1 different surface amino acid residues for [C-Mb][S_2] (Figure 5d) and [C-Lyz][S_2] (SI Figure 9), respectively. These were only slightly greater than the observed values of 2.2 ± 0.8 and 2.3 ± 0.7 in acetonitrile for the myoglobin and lysozyme constructs, respectively (Figure 5e

dx.doi.org/10.1021/ja507592b | J. Am. Chem. Soc. 2014, 136, 16824–16831

and SI Figure 9). In contrast, the number of contact points increased to 4 ± 2 for both the myoglobin and lysozyme systems in water (Figure 5f and SI Figure 9), consistent with the increased lability of S_2 in water. The above results indicated that movement of S_2 molecules across the surface of the protein was reduced concomitantly with decreases in the dielectric constant of the medium. We attributed these results to an attenuation of the electrostatic interactions in the high-dielectric medium and the predominance of hydrophobic tail burial in micellelike structures under these conditions.

CONCLUSIONS

We have demonstrated the first molecular dynamics simulations describing the structure and dynamics of surface-engineered globular proteins in aqueous, nonaqueous, and solvent-free environments. The solvent-free liquids are distinguished by closely packed arrangements of discrete protein−polymer surfactant nanoconjugates that consist of an intact globular protein core surrounded by a corona of strongly associated polymer surfactant molecules with low levels of nearest-neighbor interdigitation. The corona is structurally disordered and comprises polymer surfactant chains with moderately extended spatial conformations that are similar to the simulated structures obtained in a low-dielectric medium (acetonitrile). Inspection of the models reveals protein−protein separations of 4.5−4.8 nm and indicates that the globular protein structure is conserved throughout the simulations. Recent molecular dynamics simulations of proteins under destabilizing conditions have shown that observable changes in structure can be observed on relatively short time scales.[28,29] Particularly, Baler et al.[29] demonstrated a significant change in the structure of bovine serum albumin after 64 ns in response to low pH. Therefore, although we cannot guarantee that structural changes do not occur after longer periods, 100 ns was accepted as being an appropriate time scale on the basis of the equilibrated nature of the protein and the closeness to the experimental data.

Significantly, the simulated parameters are in close agreement with the corresponding experimental data and therefore provide validation of previous observations of structure preservation, protein dynamics, and retained biological function in solvent-free liquid proteins. In particular, given the extended conformation and negligible lability of the corona in the simulated nanoconjugate melts, it seems feasible that the aqueous-like dynamics observed experimentally in the solvent-free liquid state by EINS[19] originates from protein motions that are slaved to the coronal layer rather than from long-range movements of the polymer surfactant molecules that serve to mimic the dynamics of water molecules.

Finally, we note that the models indicate that the average head-to-tail distance of the polymer surfactant molecules in the solvent-free state is increased or decreased compared with simulations undertaken in the presence of water or acetonitrile, respectively. Thus, the coronal layer is highly responsive to the dielectric constant of the medium, and this unprecedented insight could aid significantly in predicting how molecules such as enzyme substrates and products might interact with the protein−polymer nanoconstructs when they are solubilized in aqueous or nonaqueous solvents or prepared as solvent-free soft solids or liquids.

MATERIALS AND METHODS

Preparation of Solvent-Free Liquids. Solvent-free liquids of cationized protein−polymer surfactant constructs [C-Lyz][S_2] and [C-Mb][S_2] were prepared and characterized as described previously.[17,18,21] Briefly, DMPA was coupled to the accessible acidic amino acid residues of hen egg white lysozyme (Lyz) (Sigma UK) and equine skeletal muscle myoglobin (Mb) (Sigma UK) via carbodiimide activation. After dialysis against Milli-Q water for 48 h and centrifugation, an aqueous solution of C-Lyz or C-Mb was added to an aqueous solution of S_2 (pH 6.8, 10 mg·mL^{-1}, Sigma UK; SI Figure 1), and the mixture was stirred for 12 h to produce an aqueous solution of the [C-Lyz][S_2] or [C-Mb][S_2] nanoconjugates. Unbound polymer surfactant molecules were removed by dialysis against Milli-Q water for 48 h, and the solutions were then lyophilized for 48 h. The resulting solvent-free low-density powders yielded solvent-free liquids upon thermal annealing.

Molecular Dynamics Simulations. The cationized (C-) protein−polymer surfactant (S_2) conjugates were constructed using the following procedures. The new residue types associated with the cationized amino acids were added to the AMBER99SB-ILDN force field[30] with GAFF[31] parameters generated by acpypi[32] and antechamber.[33] Force-field parameters for the S_2 ligand and heme were generated by the same methods. All of the systems had hydrogen atoms added to give protonation states consistent with pH 7. The C-protein−S_2 complexes were built using the molecular docking program BUDE[34] to dock 10 copies of the S_2 ligand at each of 26 (lysozyme) or 43 (myoglobin) randomly distributed surface points, followed by selection of a nonoverlapping set of 26 and 43 S_2 ligands, respectively, using in-house software (GA_lig_picker). Solvated (water or acetonitrile) complexes were prepared with the GROMACS utilities *editconf* and *genbox* using TIP3P water[35] or acetonitrile.[26] The solvent boxes were 2 nm larger than the protein or C-protein−S_2 complexes, and 0.1 M NaCl was added to the aqueous systems using *genion* to reproduce the experimental conditions. The boxes were relaxed by 10 000 steps of energy minimization followed by 0.2 ns of molecular dynamics at 298 K, restraining the proteins to their initial positions. Solvent-free systems were generated by placing eight copies of the C-protein−S_2 complex on a regular cubic grid in random orientations using BUDE. All of the simulations were performed under periodic boundary conditions using PME as *NPT* ensembles for 100 ns, unless otherwise stated. The solvated C-Lyz, C-Mb, [C-Lyz][S_2], and [C-Mb][S_2] systems were simulated at 298 K and 1 bar. The solvent-free boxes, each containing eight copies of [C-Lyz][S_2] and [C-Mb][S_2], were initially subjected to a pressure of 100 bar at 298 K to bring them close together and then simulated at 1 bar for a minimum of 50 ns at a temperature of 338 K to simulate the thermal annealing step. All of the molecular dynamics simulations were performed using GROMACS 4.5.5 using the high-performance computing facility at the University of Bristol Advanced Computing Research Centre.

Plots of RMSD, secondary structure, hydrogen bond counts, and solvent-accessible surface area were calculated using utilities *g_rms*, *do_dssp*, *g_hbond*, and *g_sas*, respectively (GROMACS 4.5.5). Protein−protein distances and simulation volumes in the solvent-free models were calculated using *g_dist* and *g_energy*, respectively (GROMACS 4.5.5). Plots of normalized $G(r)$ were calculated using *g_sans* (GROMACS 4.6.3). VMD (1.9.1)[36] was used for visualization and manipulation of structures.

Small-Angle Neutron Scattering. Small-angle neutron scattering experiments on solvent-free liquid [C-Lyz][S_2] and [C-Mb][S_2] were carried out at the LoQ and SANS2D beamlines at ISIS, respectively. Samples were cast as films between two-part quartz cells with path lengths of 1 mm. Scattering experiments on aqueous solutions of C-Lyz, C-Mb, [C-Lyz][S_2], and [C-Mb][S_2] were performed at the D22 beamline at Institut Laue-Langevin (ILL) in D_2O using 1 mm path length glass cuvettes. Data were fitted using Igor Pro 6.3 with the NIST NCNR SANS macro package.[37] For determination of the protein−protein separation distances in the solvent-free liquids, Gaussian distributions were fitted to the correlation peaks in the scattering profiles. Data sets obtained from the aqueous cationized

proteins were fitted to a polydisperse Gaussian sphere model. For aqueous conjugated proteins, a core−shell model was used and a repulsive screened Coulomb structure factor was applied to account for the increase in the scattering intensity in the low-Q region. It should be noted that this structure factor contribution could have also resulted from hydrophilic repulsion due to extended PEG polymer chain segments. The fits proceeded with <1% errors.

■ ASSOCIATED CONTENT

Supporting Information

Plots of RMSD, secondary structure, hydrogen bonds, solvent-accessible area, and volume against simulation time; checks of coronal interdigitation; S_2 mass spectrum; and surfactant lability for lysozyme constructs. This material is available free of charge via the Internet at http://pubs.acs.org.

■ AUTHOR INFORMATION

Corresponding Authors

s.mann@bristol.ac.uk
chawp@bristol.ac.uk

Notes

The authors declare no competing financial interest.

■ ACKNOWLEDGMENTS

We thank the ERC (Advanced Grant 266765 to S.M.) and the EPSRC (Early Career Fellowship EP/K026720/1 to A.W.P.) for financial support. We also thank the University of Bristol Advanced Computing Research Centre for access to Bluecrystal, the ISIS pulsed neutron and muon source at the Rutherford Appleton Laboratory for access to LoQ and SANS2D, and the ILL for access to D22.

■ REFERENCES

(1) Praprotnik, M.; Site, L. D.; Kremer, K. *Annu. Rev. Phys. Chem.* **2008**, *59*, 545−571.
(2) Shu, J. Y.; Panganiban, B.; Xu, T. *Annu. Rev. Phys. Chem.* **2013**, *64*, 631−657.
(3) Wang, R.; Zhang, Y.; Lu, D.; Ge, J.; Liu, Z.; Zare, R. N. *Wiley Interdiscip. Rev.: Nanomed. Nanobiotechnol.* **2013**, *5*, 320−328.
(4) Paci, E.; Gsponer, J.; Salvatella, X.; Vendruscolo, M. *J. Mol. Biol.* **2004**, *340*, 555−569.
(5) Okumura, H.; Itoh, S. G. *J. Am. Chem. Soc.* **2014**, *136*, 10549−10552.
(6) Perlmutter, J. D.; Drasler, W. J.; Xie, W.; Gao, J.; Popot, J.-L.; Sachs, J. N. *Langmuir* **2011**, *27*, 10523−10537.
(7) Martin, H. S. C.; Jha, S.; Coveney, P. V. *J. Comput. Chem.* **2014**, *35*, 692−702.
(8) Delemotte, L.; Tarek, M. *J. Membr. Biol.* **2012**, *245*, 531−543.
(9) Carpenter, T.; Bond, P. J.; Khalid, S.; Sansom, M. S. P. *Biophys. J.* **2008**, *95*, 3790−3801.
(10) Boyle, A. L.; Bromley, E. H. C.; Bartlett, G. J.; Sessions, R. B.; Sharp, T. H.; Williams, C. L.; Curmi, P. M. G.; Forde, N. R.; Linke, H.; Woolfson, D. N. *J. Am. Chem. Soc.* **2012**, *134*, 15457−15467.
(11) Fletcher, J. M.; Harniman, R. L.; Barnes, F. R. H.; Boyle, A. L.; Collins, A.; Mantell, J.; Sharp, T. H.; Antognozzi, M.; Booth, P. J.; Linden, N.; Miles, M. J.; Sessions, R. B.; Verkade, P.; Woolfson, D. N. *Science* **2013**, *340*, 595−599.
(12) Zaccai, N. R.; Chi, B.; Thomson, A. R.; Boyle, A. L.; Bartlett, G. J.; Bruning, M.; Linden, N.; Sessions, R. B.; Booth, P. J.; Brady, R. L.; Woolfson, D. N. *Nat. Chem. Biol.* **2011**, *7*, 935−941.
(13) Mu, Q.; Hu, T.; Yu, J. *PLoS One* **2013**, *8*, No. e68559.
(14) Yang, C.; Lu, D.; Liu, Z. *Biochemistry* **2011**, *50*, 2585−2593.
(15) Ge, J.; Lu, D.; Wang, J.; Yan, M.; Lu, Y.; Liu, Z. *J. Phys. Chem. B* **2008**, *112*, 14319−14324.
(16) Perriman, A. W.; Mann, S. *ACS Nano* **2011**, *5*, 6085−6091.
(17) Perriman, A. W.; Brogan, A. P. S.; Cölfen, H.; Tsoureas, N.; Owen, G. R.; Mann, S. *Nat. Chem.* **2010**, *2*, 622−626.
(18) Brogan, A. P. S.; Siligardi, G.; Hussain, R.; Perriman, A. W.; Mann, S. *Chem. Sci.* **2012**, *3*, 1839−1846.
(19) Gallat, F.-X.; Brogan, A. P. S.; Fichou, Y.; McGrath, N.; Moulin, M.; Härtlein, M.; Combet, J.; Wuttke, J.; Mann, S.; Zaccai, G.; Jackson, C. J.; Perriman, A. W.; Weik, M. *J. Am. Chem. Soc.* **2012**, *134*, 13168−13171.
(20) Sharma, K. P.; Bradley, K.; Brogan, A. P. S.; Mann, S.; Perriman, A. W.; Fermin, D. J. *J. Am. Chem. Soc.* **2013**, *135*, 18311−18314.
(21) Brogan, A. P. S.; Sharma, K. P.; Perriman, A. W.; Mann, S. *J. Phys. Chem. B* **2013**, *117*, 8400−8407.
(22) Hersleth, H.-P.; Hsiao, Y.-W.; Ryde, U.; Görbitz, C. H.; Andersson, K. K. *Biochem. J.* **2008**, *412*, 257−264.
(23) Wang, J.; Dauter, M.; Alkire, R.; Joachimiak, A.; Dauter, Z. *Acta Crystallogr., Sect. D* **2007**, *63*, 1254−1268.
(24) Barrick, D.; Hughson, F. M.; Baldwin, R. L. *J. Mol. Biol.* **1994**, *237*, 588−601.
(25) Walker, K. D.; Causgrove, T. P. *J. Mol. Model.* **2009**, *15*, 1213−1219.
(26) Grabuleda, X.; Jaime, C.; Kollman, P. A. *J. Comput. Chem.* **2000**, *21*, 901−908.
(27) Zhang, Y.; Patil, A. J.; Perriman, A. W.; Mann, S. *Chem. Commun.* **2013**, *49*, 9561−9563.
(28) Fogolari, F.; Corazza, A.; Varini, N.; Rotter, M.; Gumral, D.; Codutti, L.; Rennella, E.; Viglino, P.; Bellotti, V.; Esposito, G. *Proteins* **2011**, *79*, 986−1001.
(29) Baler, K.; Martin, O. A.; Carignano, M. A.; Ameer, G. A.; Vila, J. A.; Szleifer, I. *J. Phys. Chem. B* **2014**, *118*, 921−930.
(30) Lindorff-Larsen, K.; Piana, S.; Palmo, K.; Maragakis, P.; Klepeis, J. L.; Dror, R. O.; Shaw, D. E. *Proteins* **2010**, *78*, 1950−1958.
(31) Wang, J.; Wolf, R. M.; Caldwell, J. W.; Kollman, P. A.; Case, D. A. *J. Comput. Chem.* **2004**, *25*, 1157−1174.
(32) Sousa da Silva, A. W.; Vranken, W. F. *BMC Res. Notes* **2012**, *5*, No. 367.
(33) Wang, J.; Wang, W.; Kollman, P. A.; Case, D. A. *J. Mol. Graphics Modell.* **2006**, *25*, 247−260.
(34) McIntosh-Smith, S.; Price, J.; Sessions, R. B.; Ibarra, A. A. *Int. J. High Perform. Comput. Appl.* **2014**, DOI: 10.1177/1094342014528252.
(35) Jorgensen, W. L.; Chandrasekhar, J.; Madura, J. D.; Impey, R. W.; Klein, M. L. *J. Chem. Phys.* **1983**, *79*, 926−935.
(36) Humphrey, W.; Dalke, A.; Schulten, K. *J. Mol. Graphics* **1996**, *14*, 33−38.
(37) Kline, S. R. *J. Appl. Crystallogr.* **2006**, *39*, 895−900.